Axisymmetric Modes of Rotating Relativistic Stars in the Cowling Approximation

José A. Font[1], Harald Dimmelmeier[1], Anshu Gupta[2] and Nikolaos Stergioulas[3]

[1]Max-Planck-Institut für Astrophysik
Karl-Schwarzschild-Str. 1, D-85741, Garching, Germany
[2]Raman Research Institute
C.V. Raman Avenue, Sadashivanagar, Bangalore 560080, India
[3]Department of Physics, Aristotle University of Thessaloniki
Thessaloniki 54006, Greece

e-mail: font@mpa-garching.mpg.de
e-mail: harrydee@mpa-garching.mpg.de
e-mail: anshu@rri.res.in
e-mail: niksterg@astro.auth.gr

Abstract

Axisymmetric pulsations of rotating neutron stars can be excited in several scenarios, such as core-collapse, crust and core-quakes and binary mergers and could become detectable either in gravitational waves or high-energy radiation. Here, we present a comprehensive study of all low-order axisymmetric modes of uniformly and rapidly rotating relativistic stars. Initial stationary configurations are appropriately perturbed and are numerically evolved using an axisymmetric, nonlinear relativistic hydrodynamics code, assuming time-independence of the gravitational field (Cowling approximation). The simulations are performed using a high-resolution shock-capturing finite-difference scheme accurate enough to maintain the initial rotation law for a large number of rotational periods, even for stars at the mass-shedding limit. Through Fourier transforms of the time evolution of selected fluid variables, we compute the frequencies of quasi-radial and non-radial modes with spherical harmonic indices $l = 0, 1, 2$ and 3, for a sequence of rotating stars from the non-rotating limit to the mass-shedding limit. The frequencies of the axisymmetric modes are affected significantly by rotation only when the rotation rate exceeds about 50% of the maximum allowed. As expected, at large rotation rates, apparent mode crossings between different modes appear. In addition to the above modes, several axisymmetric inertial modes are also excited in our numerical evolutions.

Key words Hydrodynamics — relativity — methods: numerical — stars: neutron — stars: oscillations — stars: rotation

1 Introduction

The pulsations of rotating neutron stars are expected to be a source of detectable gravitational waves. Additionally, their excitation could become detectable in the emission of high-energy radiation. In particular, axisymmetric oscillations can be excited in a number of different astrophysical scenarios, namely: a) after a core-collapse leading to a supernova explosion (see e.g. Mönchmeyer et al 1991; Zwerger & Müller 1997), b) during starquakes induced by the secular spin-down of a pulsar, c) after a large thermonuclear explosion in the crust of an accreting neutron star, d) during a core-quake due to a large phase-transition to, for example, strange quark matter (Cheng & Dai 1998), and e) in the delayed collapse of the merged object in a binary neutron star merger (Ruffert, Janka & Schäfer 1996; Shibata & Uryu 2000). The observational detection of such pulsations will yield valuable information about the equation of state of relativistic stars (see Kokkotas, Apostolatos & Andersson, 2000, see also Kokkotas and Schmidt 1999, for a recent review on oscillations of relativistic stars).

Numerical simulations of some of these scenarios are available and provide very detailed information of the dynamics of the neutron star pulsations. In particular, the axisymmetric core-collapse simulations of Mönchmeyer et al (1991) and Zwerger & Müller (1997), revealed that, after the collapse and bounce of an iron core, the unshocked inner core (the proto-neutron star) oscillates with various volume (radial and quasi-radial) and surface modes. The amplitude and frequency of these fluid modes (f- and p-modes) was found to depend on the kinetic energy of the inner core at bounce, the stiffness of the equation of state (EOS), and the central and average density of the inner core. These authors found that the amplitude of the post-bounce oscillations is small for spherical models, being strongly damped through the emission of asymmetric pressure waves, in time scales of the order of 1ms. However, for rotating cores which bounce due to centrifugal forces at subnuclear densities, much larger amplitudes are achieved (as large as 10 times the central density) and the damping time scale becomes comparable to the oscillation time scale ($\gg$ 1ms). Recently, Dimmelmeier, Font & Müller (2000) have developed a code to study axisymmetric core-collapse in general relativity using the conformally flat metric approach (Wilson, Mathews & Marronetti 1996). This code is currently being applied to collapse some of the initial models of Zwerger & Müller (1997), to analyze the gravitational waves emitted in the process. Excitation of axisymmetric modes have already been observed in such relativistic core-collapse simulations.

Of all axisymmetric modes, the quasi-radial modes of slowly-rotating relativistic stars were first studied by Hartle & Friedman (1975) and, more recently, by Datta et al. (1998). In rapid rotation, quasi-radial modes of relativistic stars have been studied by Yoshida & Eriguchi (2000) in the Cowling approximation (McDermott, Van Horn & Scholl 1983), i.e., by neglecting the perturbations in the gravitational field (see Stergioulas 1998 for a recent review on the equilibrium structure and oscillations of rapidly rotating stars in general relativity). For Newtonian stars, axisymmetric modes have been extensively studied by Clement (1981, 1984, 1986). From the above studies, it has become apparent that rotation weakly modifies the oscillation frequencies for low-order modes, but introduces apparent crossings between higher-order modes for rapidly rotating models. In addition, in Clement (1981) it is claimed that the axisymmetric quadrupole f-mode lies on a continuous branch for rapidly rotating Newtonian stars.

In this paper we compute all low-order l = 0, 1, 2 and 3 axisymmetric modes for rapidly rotating stars in general relativity, in the Cowling approximation. For this purpose, we use a 2-D nonlinear hydrodynamics code, whose accuracy has been extensively tested in Font, Stergioulas &

Kokkotas (2000) (hereafter FSK; see also Stergioulas, Font & Kokkotas 1999). This code is based on high-resolution shock-capturing (HRSC) finite-difference schemes for the numerical integration of the general relativistic hydrodynamic equations (see Font 2000 for a recent review). We note in passing that the 3-D version of the numerical methods employed here has been recently applied by Stergioulas & Font (2000) in the study of the large-amplitude, nonlinear evolutions of r-modes in rotating relativistic stars. In our present study of axisymmetric modes, we focus on a sequence of equilibrium models with a polytropic ($N = 1.0$) equation of state and uniform rotation. For the excitation of the various oscillation modes, low-amplitude perturbations (using appropriate trial eigenfunctions) are added to the initial equilibrium models. The Cowling approximation allows us to evolve relativistic matter for a much longer time than presently available coupled spacetime plus hydrodynamical evolution codes (Alcubierre et al. 2000; Font et al. 2000; Shibata, Baumgarte & Shapiro 2000; Shibata & Uryu 2000). This is particularly evident when hydrodynamically evolving rotating stars. Nevertheless, since pulsations of neutron stars are mainly a hydrodynamical process, the approximation of a time-independent gravitational field still allows for qualitative conclusions to be drawn, when studying the evolution of perturbed rotating neutron stars. In addition, our present results will serve as test-beds for 3-D general-relativistic evolution codes.

The paper is organized as follows: In Section 2 we describe the setup of the problem, by briefly presenting some details of the initial equilibrium stellar configurations and the main features of the hydrodynamical code. In Section 3 we explain the procedure by which the initial equilibrium models are perturbed. Section 4 presents the main results of our simulations, including the frequencies of all low-order axisymmetric modes for our sample of initial models. The paper ends with Section 5 where a summary is presented, together with an outlook of possible future directions of this investigation.

2 Problem Setup

Our initial models are exact, numerical solutions of rapidly rotating relativistic stars, having uniform angular velocity Ω. We assume a perfect fluid, zero-temperature equation of state (EOS), for which the energy density is a function of pressure only. The following relativistic generalization of the Newtonian polytropic EOS is chosen:

$$p = K\rho_0^{1+1/N}, \tag{1}$$

$$\epsilon = \rho_0 + Np, \tag{2}$$

where p is the pressure, ϵ is the energy density, ρ_0 is the rest-mass density, K is the polytropic constant and N is the polytropic exponent. The initial equilibrium models are computed using a numerical code developed by Stergioulas & Friedman (1995). Our representative neutron star models are characterized by $N = 1$, $K = 100$ and central density $\rho_C = 1.28 \times 10^{-3}$, in units in which $c = G = M_\odot = 1$. We compute 12 different initial models by varying the polar to equatorial circumferential radius from 1 (non-rotating star) to 0.65 (near the mass-shedding limit), as listed in Table 1. The angular velocity at the mass-shedding limit is $\Omega_K = 0.8094 \times 10^4$ s^{-1} for this sequence of rotating relativistic stars of same central density. In order to be able to study stellar pulsations the initial model is supplemented by a uniform, non-rotating "atmosphere" of very low density, typically 10^{-6} or less times the central density of the star (see related discussion in FSK).

The initial data are subsequently evolved in time with a hydrodynamics code. The (axisymmetric) hydrodynamic equations are written as a first-order flux-conservative system which expresses the conservation laws of mass, momentum and energy. The specific form of the equations was presented in FSK and we will not repeat it here. These equations are solved using a HRSC finite-difference scheme (Font 2000). A comprehensive description of the specific numerical techniques we employ was previously reported in FSK. Therefore, we only mention here that the code makes use of the third-order piecewise parabolic method, PPM (Colella & Woodward 1984), for the cell-reconstruction procedure, together with Marquina's flux-formula (Donat et al 1998) to compute the numerical fluxes. The PPM reconstruction scheme was shown to be accurate enough for maintaining the initial rotation laws during many rotational periods.

The hydrodynamic equations are implemented in the code using spherical polar coordinates (r, θ, ϕ) and assuming axisymmetry, i.e., all derivatives with respect to the ϕ coordinate vanish. The radial computational domain extends to 1.2 times the radius of the star (the 20% additional zones are used for the atmosphere). In the polar direction, the selected domain depends on the spherical harmonic index of the pulsation modes: for even l modes the domain extends from $\theta = 0$ (pole) to $\theta = \pi/2$ (equator). For odd l modes, the domain extends to $\theta = \pi$. The number of grid points we employ is 200×80 for l being even and 160×120 for l being odd, in r and θ respectively. The boundary conditions are implemented in the same way as in FSK.

Our numerical evolution code was thoroughly tested in FSK, by comparing evolutions of perturbed spherical stars with results from perturbation theory obtained with an independent eigenvalue code. Since then, the code has been upgraded to run efficiently on a NEC SX-5/3C vector supercomputer. This modification was essential for doing a large number of numerical evolutions for many rotational periods and with a large number of grid-points.

3 Perturbation of the Initial Data

The accurate computation of mode frequencies in a rotating star requires an appropriate excitation of the equilibrium initial data. When doing so, it is possible to obtain the frequencies of the excited modes with good accuracy, through a Fourier transform of the time evolution of the hydrodynamical variables, provided that the evolution time is much larger than the period of oscillations. As in the hydrodynamical evolution we are using the 3+1 formulation (Banyuls et al 1997), the oscillation frequencies of the various evolved variables are obtained with respect to the coordinate time at a given location. This corresponds to the frequency of oscillations in a reference frame attached to an inertial observer at infinity. To increase the accuracy in the computation of the frequencies, we search for the zeros of the first derivative of the Fourier transform (with respect to the frequency), using second-order accurate central differences. These zeros correspond to maxima in the Fourier transform, which (except for high-frequency noise) correspond to the excited modes of oscillation. This procedure is done at several points inside the star and the frequencies thus determined are found to be the same for each mode, i.e., all the modes that we identify are global discrete modes. For the resolution employed we estimate the accuracy of the computed frequencies to be of the order of $1\% - 2\%$. The different pulsation frequencies are identified with specific normal modes by comparing frequencies of the non-rotating star to known eigenfrequencies from perturbative normal-mode calculations.

As demonstrated in FSK, the small-amplitude pulsations in the nonlinear, fixed spacetime evolutions correspond to linear normal modes of pulsation in the relativistic Cowling approximation (McDermott et al 1983), in which perturbations of the spacetime are ignored. The existence of a numerical viscosity inherent to the numerical scheme, damps the pulsations of the star – together with the presence of a constant-density atmosphere. Hence, high-resolution grids are preferred to minimize this effect, especially for the higher frequency modes, which are damped faster.

We use analytic eigenfunctions to excite particular oscillation modes. For the $l = 0$ modes the initial equilibrium values of density and pressure, ρ_0 and p_0, are perturbed to nonequilibrium values, $\rho = \rho_0 + \delta\rho$ and $p = p_0 + \delta p$ by the eigenfunctions

$$\delta\rho = A\rho_c \sin\left(\frac{\pi r}{r_s(\theta)}\right), \tag{3}$$

$$\delta p = \Gamma p_i \frac{\delta\rho}{\rho_i}, \tag{4}$$

where ρ_c is the central density, $r_s(\theta)$ is the coordinate radius of the surface of the star (which depends on the polar angle θ) and Γ is the adiabatic index of the ideal gas EOS, $p = (\Gamma - 1)\rho\epsilon$, related to the polytropic index by the equation $\Gamma = 1 + 1/N$ (for isentropic stars). The amplitude of the excitation, A, is typically chosen to be in the range 0.001 to 0.005.

For the excitation of the $l = 1, 2$ and 3 modes we add a small non-zero θ-velocity component to perturb the initial vanishing value. More precisely, for $l = 1$ we have

$$v_\theta = A \sin\left(\frac{\pi r}{r_s(\theta)}\right) \sin\theta, \tag{5}$$

for $l = 2$

$$v_\theta = A \sin\left(\frac{\pi r}{r_s(\theta)}\right) \sin\theta\cos\theta, \tag{6}$$

and for $l = 3$

$$v_\theta = A \sin\left(\frac{\pi r}{r_s(\theta)}\right) \sin\theta(1 - 5\cos^2\theta). \tag{7}$$

The particular radial dependence in the above eigenfunctions is chosen so that the perturbations vanish at the surface of the rotating star. We have found that this is necessary for our numerical scheme to work. Figure 1 displays a 2-D greyscale plot of the above perturbations, for the model near the mass-shedding limit. The darkest area corresponds to the maximum of the perturbation, while the lightest area corresponds to its minimum values. We note that all models have equatorial plane symmetry with respect to the $z = 0$ axis, even though we use a grid extending to $\theta = \pi$ for odd l's. The choice of these trial eigenfunctions allows us to compute the four lowest frequencies quite accurately for all the considered l modes, as we discuss next.

4 Results

We turn now to presenting our numerical results concerning the frequencies of axisymmetric pulsations of uniformly and rapidly rotating neutron stars.

4.1 Quasi-radial modes

Figure 2 shows the time evolution of the radial velocity component for the most rapidly rotating model in our sequence. The initial equilibrium model has been perturbed with an $l = 0$ perturbation according to Eqs. (3) and (4). The final evolution time corresponds to 10ms and the oscillations are measured at half the radius of the star and at an angle of $\theta = \pi/4$. The oscillatory pattern depicted in this figure is typical to all our simulations: it is mainly a superposition of the lowest-order normal modes of the fluid. The amplitude of the oscillations is damped due to the inherent viscosity of the numerical scheme. The high frequency normal modes are usually damped faster and at the final time the star is pulsating mostly in a few lowest frequency modes.

The frequencies of the axisymmetric modes are obtained by a Fast Fourier Transform of the time evolution of selected hydrodynamical variables (both the density and the components of the velocity). Figure 3 shows the Fourier transform of the radial velocity evolution depicted in Fig. 2. The main mode which is excited is the fundamental quasi-radial F-mode. Its higher harmonics ($H1$-$H3$) are also excited, as well as several other, non-radial modes. The amount of excitation of each mode depends on the correlation between the mode eigenfunction and the applied perturbation.

As it is apparent in Figure 3, a dense spectrum of modes appears when one applies generic perturbations that do not correspond to the eigenfunctions of a particular normal mode only. Thus, in order to identify the peaks in the Fourier transform with specific normal modes, we rely on the previously known frequencies in the non-rotating limit (see FSK). As the rotation rate is increased, we follow the change in the location of the various peaks, keeping in mind that at large rotation rates apparent crossings of frequencies occur. In such a case, the amplitude of the Fourier transform at various points inside the star (which correlates with the mode eigenfunction) is used as a guide in deciding about the correct identification of the mode frequency. The specific values for the frequencies of the fundamental F and higher harmonics H_1, H_2, H_3 quasi-radial modes for the sequence of rotating stars considered here, are shown in Table 2.

As frequencies of quasi-radial modes have been computed previously by Yoshida & Eriguchi (2000), as an eigenvalue problem, we use those results to compare the values obtained with our code for a soft polytrope, with $\rho_{\rm c} = 8.1 \times 10^{-4}$, $N = 1.5$ and $K = 4.349$. We have compared the models corresponding to $\Omega = 0, 7.1379 \times 10^{-3}$ and 1.4094×10^{-2}, which, in the notation of Yoshida & Eriguchi correspond to $f_{\rm rot} = 0, 0.1415$ and 0.2794, respectively. The results of this comparison are presented in Table 3. We note that the agreement is very good, especially for the most rapidly rotating model, the differences always being below 2%. As there may be some small differences in the construction of the equilibrium model, the actual accuracy of our code is better than the relative differences shown in Table 3.

4.2 Non-radial modes

In Figures (4-9) we plot the time evolutions of the polar velocity component, along with the corresponding Fourier transforms for non-radial $l = 1, 2$ and 3 perturbations, for the fastest rotating model in Table 1. The time evolutions shown are measured at half the star radius and $\theta = 2\pi/3$ for $l = 1, 3$, and $\theta = \pi/3$ for $l = 2$. The above time evolutions show the same qualitative behavior already described for the $l = 0$ modes. For $l = 1$, the dominant frequency is the fundamental mode ${}^1f$, even at early times, which shows that the perturbation applied to excite the $l = 1$ modes is very close to the ${}^1f$ eigenfunction.

For $l = 2$, a larger number of modes is excited by the initial perturbation. At late times, the evolution is mainly a superposition of the fundamental ${}^2f$-mode and the fundamental quasi-radial F-mode, as it is evident from the amplitudes of the various modes in the corresponding Fourier transform.

For $l = 3$, a large number of modes is also excited by the initial perturbation, as in the $l = 2$ case. At late times, the evolution is mainly a superposition of the fundamental ${}^3f$- and ${}^1f$-modes and of the fundamental quasi-radial F-mode. The Fourier amplitude of the ${}^1f$-mode is larger than the amplitude of the ${}^3f$-mode, which shows that the eigenfunction of the $l = 3$ modes near the mass-shedding limit is significantly modified by rotation, so that the $l = 3$ part of the ${}^1f$-eigenfunction correlates better with the generic eigenfunction we used to excite $l = 3$ modes, than the ${}^3f$-eigenfunction itself.

The frequencies of all identified $l = 1, 2$ and 3 modes are displayed in detail in Tables 4-6. The modes are labeled as ${}^lf$ for the fundamental modes and ${}^lp_n$ for the p-modes of order n. A plot of all mode-frequencies as a function of the rotation rate is shown in Figure 10. At rotation rates below $\sim 50\%$ of the mass-shedding limit, the frequencies of the lowest-order modes are not significantly affected by rotation. This is consistent with previous results in the slow-rotation approximation (Hartle & Friedman 1975) and in the Newtonian limit. For larger rotation rates, however, the $l = 0$ and $l = 1$ overtones have a tendency to increase in frequency with rotation rate, while the $l = 2$ and $l = 3$ overtones have the opposite tendency. As a result, several apparent mode crossings take place between different modes. This has been observed before by Clement (1986) for Newtonian axisymmetric modes and by Yoshida & Eriguchi (2000) for the relativistic quasi-radial modes.

In the above studies, when one follows an eigenfrequency continuously from the non-rotating limit to the large rotation rates, then, at apparent mode crossings, the continuous lines corresponding to different frequency sequences do not cross, which is normally called "avoided crossing". Such avoided crossings can occur in two ways: the eigenfunction along a continuous frequency sequence remains that of the same mode (which is the usual type of avoided crossing in non-rotating stars, see Unno et al 1989) or a different mode appears in the same continuous frequency sequence after the avoided crossing. The latter case is encountered in rotating stars, as in Figure 10. To distinguish the two cases, we prefer to use the term "apparent crossing" for rotating stars (as was done in Clement 1986), which refers to a mode-sequence, rather than a frequency sequence.

Finally, we note that in Clement (1981) it is claimed that the axisymmetric ${}^2f$-mode lies on a continuous branch, near the mass-shedding limit, for rapidly rotating Newtonian stars. In our relativistic computation, no such behavior was found for any of the modes studied. Within the numerical resolution employed all identified modes were found to be discrete.

4.3 Inertial modes

Apart from the quasi-radial and f- and p-modes, a number of axisymmetric inertial modes was also excited in our numerical evolutions, which can be seen as low-frequency peaks in our Fourier transforms (Figures 3-9). These modes exist in isentropic stars (such as those considered here) as a mixture of axial r-modes and polar g-modes (see Lockitch & Friedman 1999). Nonaxisymmetric inertial modes have been computed as an eigenvalue problem for slowly-rotating relativistic stars (Lockitch 1999, Lockitch, Andersson & Friedman 2000), but frequencies for axisymmetric modes are not available yet. This makes their identification difficult, as, in our simulations, many modes with similar frequencies appear. Furthermore, the spacing between these frequencies is of the same order as one would expect the difference between the relativistic frequencies and the Newtonian frequencies (computed in Lockitch & Friedman 1999) to be. Therefore, it would be too venturous, at this point, to attempt an identification with specific normal modes, without prior knowledge of some of these frequencies in relativity, at least for slow-rotation.

5 Summary and Outlook

We have presented a comprehensive study of all low-order axisymmetric modes of uniformly and rapidly rotating relativistic stars in the Cowling approximation. This investigation has been carried out by numerically evolving initial perturbed equilibrium configurations with an axisymmetric, nonlinear, relativistic hydrodynamics code. The simulations were performed using a high-resolution shock-capturing finite-difference scheme accurate enough to maintain the initial rotation law for a sufficient number of rotational periods.

Through Fourier transforms of the time evolution of selected fluid variables we computed the frequencies of non-radial, axisymmetric modes (with angular momentum indices $l = 0, 1, 2$ and 3) of rapidly rotating stars. Therefore, we have extended previous results by Yoshida & Eriguchi (2000) which were mainly restricted to quasi-radial modes. We have presented results for a complete sequence of rotating stars, ranging from the non-rotating case to rapid rotation near the mass-shedding limit. Apparent crossings between different modes appear for rapidly rotating stars, as a result of the different influence of rotation on quasi-radial and $l = 1$ modes than on modes with $l \geq 2$. This different behavior may be related to the fact that the rotational deformation of the equilibrium star appears first as an $l = 2$ term. Several axisymmetric inertial modes were also excited in our simulations. However, a definitive identification of the observed frequency peaks with specific modes will only be possible when mode-frequencies on the slow-rotation approximation be computed as an eigenvalue problem. Alternatively, a determination of mode-eigenfunctions in our simulations (and a comparison to mode-eigenfunctions in the Newtonian limit) may also allow the identification of such inertial modes.

In following work we plan to study axisymmetric modes of differentially rotating stars with realistic equations of state. Moreover, the implementation of the hydrodynamic equations and numerical techniques employed in the present work has been recently extended (Dimmelmeier et al 2000) to allow for gravitational field dynamics through the so-called *conformally flat metric* approach (Wilson et al 1996). Studies of fully coupled evolutions with such a code, in the context of pulsations of rotating relativistic stars, will be presented elsewhere.

Acknowledgements

We thank John Friedman, Kostas Kokkotas and Ewald Müller for helpful discussions and comments on the manuscript. All computations have been performed on a NEC SX-5/3C Supercomputer at the Rechenzentrum Garching. A.G. thanks the Max-Planck-Institut für Gravitationsphysik, Golm and the Max-Planck-Institut für Astrophysik, Garching, for supporting a visit during which this collaboration was initiated. This research was supported in part by the European Union grant HPRN-CT-2000-00137.

References

[1] Alcubierre M., Brügmann B., Dramlitsch T., Font J.A., Papadopoulos P., Seidel E., Stergioulas N., Takahashi R., 2000, Phys. Rev. D, 62, 044034

[2] Banyuls F., Font J.A., Ibáñez J.M., Martí J.M., Miralles J.A., 1997, ApJ, 476, 221

[3] Cheng K.S., Dai Z.G., 1998, ApJ, 492, 281

[4] Clement M.J., 1981, ApJ, 249, 746

[5] Clement M.J., 1984, ApJ, 276, 724

[6] Clement M.J., 1986, ApJ, 301, 185

[7] Colella P., Woodward P.R., 1984, J. Comput. Phys., 54, 174

[8] Datta B., Hasan S.S., Sahu P.K., Prasanna A.R., 1998, Int. J. Mod. Phys. D, 7, 49

[9] Dimmelmeier H., Font J.A., Müller E., 2000, in *Gravitational waves: a challenge to theoretical astrophysics*, ICTP Lecture Notes Series, in press

[10] Donat R., Font J.A., Ibáñez J.M., Marquina A., 1998, J. Comput. Phys., 146, 58

[11] Font J.A., Stergioulas N., Kokkotas K.D., 2000, MNRAS, 313, 678 (FSK)

[12] Font J.A., Miller M., Suen W.-M., Tobias M., 2000, Phys. Rev. D, 61, 044011

[13] Font J.A., 2000, Living Rev. Relativ., 2000-2 (`http://www.livingreviews.org/Articles/Volume3/2000-2font/`)

[14] Hartle J.B., Friedman J.L., 1975, ApJ, 196, 653

[15] Kokkotas K.D., Apostolatos Th., Andersson, N., 2000, MNRAS, in press

[16] Kokkotas K.D., Schmidt, B.G., 1999, Living Rev. Relativ., 1999-2 (`http://www.livingreviews.org/Articles/Volume3/1999-2kokkotas/`)

[17] Lockitch K.H., 1999, Ph.D. Thesis, University of Wisconsin-Milwaukee, gr-qc/9909029

[18] Lockitch K.H., Friedman J.F., 1999, ApJ, 521, 764

[19] Lockitch K.H., Andersson, N., Friedman J.F., 2000, gr-qc/0008019

[20] McDermott P.N., Van Horn H.M., Scholl J.F., 1983, ApJ, 268, 837

[21] Mönchmeyer R., Schäffer G., Müller E., Kates R.E., 1991, A&A, 246, 417

[22] Ruffert M., Janka H.-Th., Schäfer G., 1996, A&A, 311, 532

[23] Shibata M., Baumgarte Th.W., Shapiro S.L., 2000, Phys. Rev. D, 61, 044012

[24] Shibata M., Uryu K., 2000. Phys. Rev. D, 61, 064001

[25] Stergioulas N., Friedman J.L., 1995, ApJ, 444, 306

[26] Stergioulas N., 1998, Living Rev. Relativ., 1998-8 (`http://www.livingreviews.org/Articles/Volume1/1998-8stergio/`)

[27] Stergioulas N., Font J.A., Kokkotas K.D., 1999, Proceedings of the 19th Texas Symposium on Relativistic Astrophysics, in press (gr-qc/9904009)

[28] Stergioulas N., Font J.A., 2001, Phys. Rev. Lett., in press (gr-qc/0007086)

[29] Unno W., Osaki Y., Ando H., Saio H., Shibahashi H., 1989, *Nonradial Oscillations of Stars*, University of Tokyo Press

[30] Wilson J.R., Mathews G.J., Marronetti P., 1996, Phys. Rev. D, 54, 1317

[31] Yoshida S., Eriguchi Y., 2001, MNRAS, in press (astro-ph/9908359)

[32] Zwerger T., Müller E., 1997, A&A, 320, 209

Table 1: Equilibrium properties of the initial models, as described by a polytropic EOS, $p = K\rho_0^{1+1/N}$, where $N = 1$, $K = 100$ and with central rest-mass density $\rho_C = 1.28 \times 10^{-3}$ (in units with $c = G = M_\odot = 1$). The entries in the table are as follows: Ω is the angular velocity of the star, M and M_0 are the gravitational and rest mass, T/W is the ratio of rotational to gravitational binding energy and R is the equatorial circumferential radius.

Ω ($10^4 s^{-1}$)	M ($\mathrm{M}_\odot$)	M_0 ($\mathrm{M}_\odot$)	T/W ($\times 10^{-2}$)	R (km)
0.0	1.400	1.506	0.0	14.15
0.218	1.432	1.541	1.200	14.51
0.306	1.466	1.579	2.438	14.92
0.371	1.503	1.619	3.701	15.38
0.399	1.523	1.641	4.339	15.63
0.423	1.543	1.663	4.976	15.91
0.445	1.564	1.686	5.609	16.21
0.465	1.585	1.709	6.232	16.52
0.482	1.607	1.733	6.839	16.87
0.498	1.627	1.756	7.419	17.25
0.511	1.647	1.778	7.959	17.68
0.522	1.666	1.798	8.439	18.15

Table 2: Fundamental, first, second and third overtones (F, H_1, H_2 and H_3, respectively) of the quasi-radial ($l = 0$) modes for a sequence of rotating stars of same central density. The angular velocity Ω_K at the mass-shedding limit is 0.8094×10^4 s^{-1} for this sequence.

Ω ($10^4 s^-1$)	F (kHz)	H_1 (kHz)	H_2 (kHz)	H_3 (kHz)
0.0	2.706	4.547	6.320	8.153
0.218	2.657	4.467	6.215	8.005
0.306	2.619	4.409	6.202	8.005
0.371	2.579	4.385	6.234	8.096
0.399	2.553	4.377	6.243	8.098
0.423	2.535	4.371	6.241	8.134
0.445	2.510	4.362	6.266	8.171
0.465	2.495	4.356	6.262	8.171
0.482	2.476	4.366	6.274	8.197
0.498	2.456	4.357	6.270	8.130
0.511	2.442	4.350	6.297	8.030
0.522	2.417	4.337	6.255	7.987

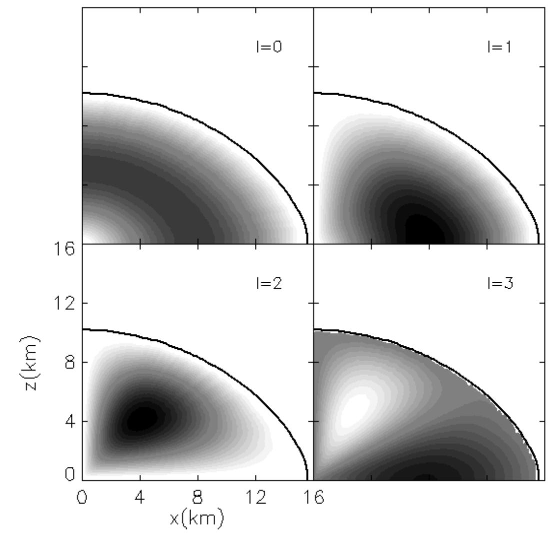

Figure 1: 2-D greyscale plot of the initial data used for mode-excitation: density perturbation ($l = 0$) and v_θ ($l \neq 0$). The darkest area corresponds to the maximum of the perturbation, while the lightest area corresponds to its minimum values. The thick solid line indicates the location of the surface of the star. The depicted initial model is the fastest rotator of our sample in Table 1.

Table 3: Comparison of $l = 0$ quasi-radial pulsation frequencies, obtained with the present nonlinear evolution code, to linear perturbation mode frequencies in the relativistic Cowling approximation (Yoshida & Eriguchi 2000). The equilibrium model is a $N = 1.5$, $K = 4.349$ relativistic polytrope with $\rho_C = 8.1 \times 10^{-4}$.

Ω (10^{-3})	Mode	Y&E (kHz)	present (kHz)	Difference (per cent)
0	F	1.674	1.678	0.3
	H1	2.758	2.807	1.7
	H2	3.793	3.841	1.3
7.1379	F	1.646	1.670	1.5
	H1	2.696	2.735	1.4
	H2	3.728	3.761	0.9
14.094	F	1.545	1.553	0.5
	H1	2.572	2.595	0.9
	H2	3.664	3.642	0.6

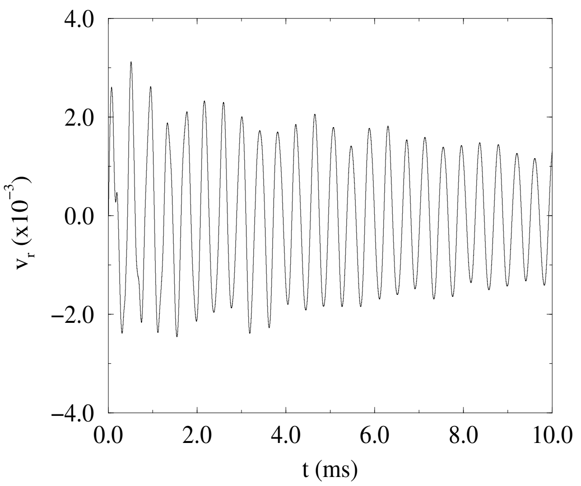

Figure 2: Time evolution of the radial velocity of the most rapidly rotating model of our sequence, $\Omega = 0.522 \times 10^4 s^{-1}$. An $l = 0$ perturbation has been applied to the equilibrium data. The pulsations are mainly a superposition of the normal modes of the star.

Table 4: f-mode and first three p-modes corresponding to $l = 1$. Further details in Tables 1 and 2.

Ω ($10^4 s^-1$)	^1f (kHz)	$^1p_1$ (kHz)	$^1p_2$ (kHz)	$^1p_3$ (kHz)
0.0	1.335	3.473	5.335	7.136
0.218	1.349	3.464	5.318	7.134
0.306	1.356	3.453	5.317	7.152
0.371	1.364	3.446	5.320	7.172
0.399	1.369	3.442	5.322	7.193
0.423	1.371	3.438	5.325	7.214
0.445	1.373	3.434	5.328	7.238
0.465	1.375	3.429	5.333	7.223
0.482	1.376	3.422	5.339	7.349
0.498	1.376	3.417	5.340	7.288
0.511	1.375	3.407	5.337	7.281
0.522	1.375	3.393	5.335	7.318

Table 5: f-mode and first three p-modes corresponding to $l = 2$. Further details in Tables 1 and 2.

Ω ($10^4 s^-1$)	^2f (kHz)	$^2p_1$ (kHz)	$^2p_2$ (kHz)	$^2p_3$ (kHz)
0.0	1.846	4.100	6.019	7.867
0.218	1.855	4.040	5.910	7.684
0.306	1.860	3.944	5.716	7.471
0.371	1.857	3.814	5.521	7.264
0.399	1.851	3.734	5.431	7.130
0.423	1.844	3.645	5.325	7.000
0.445	1.832	3.554	5.226	6.989
0.465	1.815	3.456	5.164	6.970
0.482	1.787	3.352	4.962	6.823
0.498	1.762	3.244	4.810	6.746
0.511	1.733	3.120	4.822	6.653
0.522	1.686	3.010	4.726	6.571

Table 6: f-mode and first three p-modes corresponding to $l = 3$. Further details in Tables 1 and 2.

Ω $(10^4 s^{-1})$	${}^3f$ (kHz)	${}^3p_1$ (kHz)	${}^3p_2$ (kHz)	${}^3p_3$ (kHz)
0.0	2.228	4.622	6.635	8.600
0.218	2.228	4.570	6.550	8.418
0.306	2.221	4.485	6.433	8.304
0.371	2.199	4.380	6.280	8.109
0.399	2.186	4.330	6.214	8.105
0.423	2.177	4.303	6.135	8.000
0.445	2.148	4.194	6.067	7.831
0.465	2.118	4.124	5.987	7.751
0.482	2.094	4.044	5.895	7.751
0.498	2.055	3.964	5.784	7.656
0.511	2.017	3.870	5.852	7.612
0.522	1.965	3.720	5.767	7.593

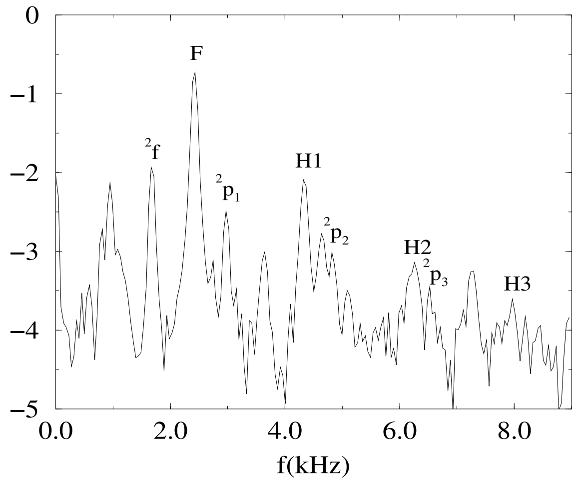

Figure 3: Logarithm of the amplitude (in arbitrary scale) resulting from the Fourier transform of the radial velocity evolution shown in Fig. 2. It is possible to identify in this plot the frequencies of the fundamental quasi-radial mode as well as up to three harmonics. Additionally, f and overtones of $p-$modes can also be identified.

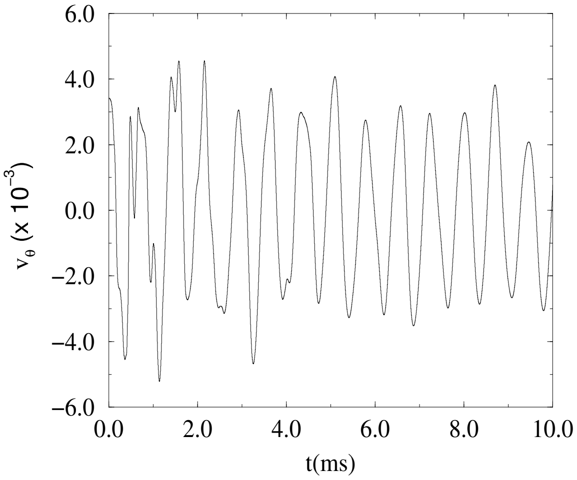

Figure 4: Time evolution of the polar velocity component for the fastest rotator, $\Omega = 0.522 \times 10^4 s^{-1}$. An $l = 1$ perturbation has been applied to the equilibrium data.

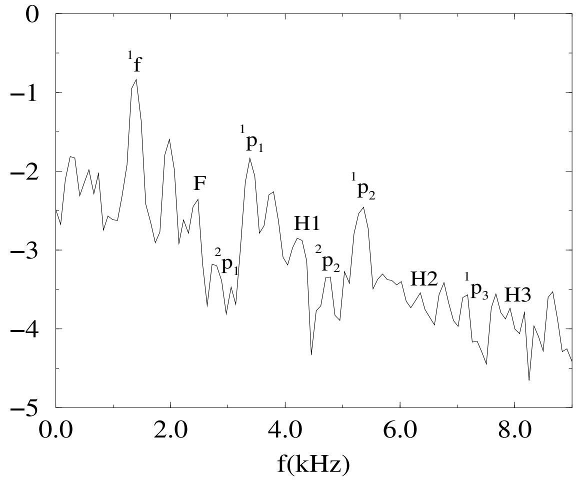

Figure 5: Fourier transform of the polar velocity evolution shown in Fig. 4. The different axisymmetric, $l = 1$ modes are conveniently labelled.

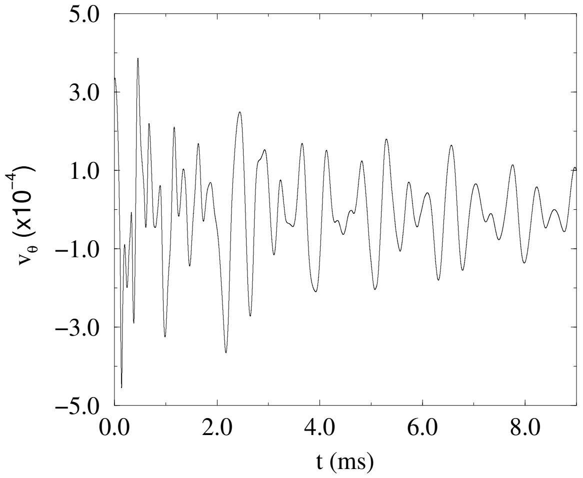

Figure 6: Same as Fig. 4 but showing the time evolution for the $l = 2$ perturbation.

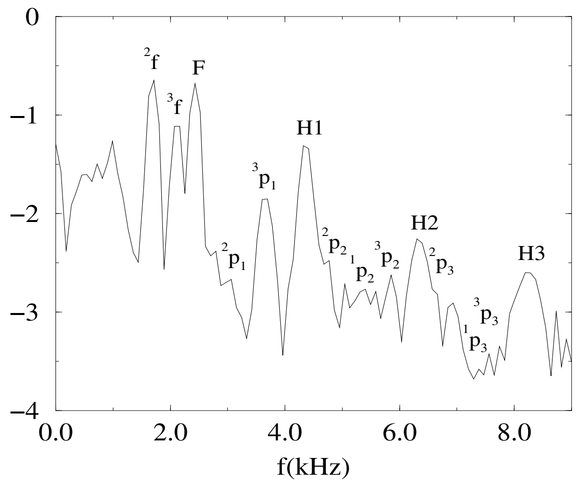

Figure 7: Same as Fig. 5 but showing the frequencies of the $l = 2$ axisymmetric modes.

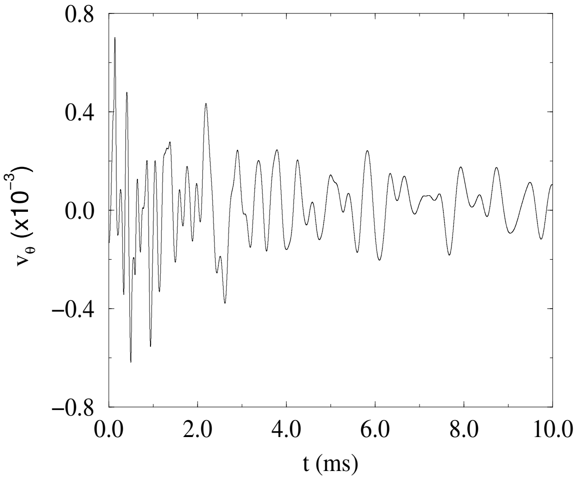

Figure 8: Same as Fig. 4 but showing the time evolution for the $l = 3$ perturbation.

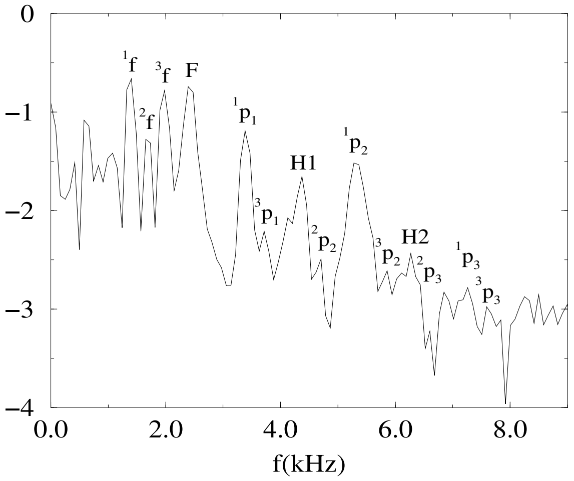

Figure 9: Same as Fig. 5 but showing the frequencies of the $l = 3$ axisymmetric modes.

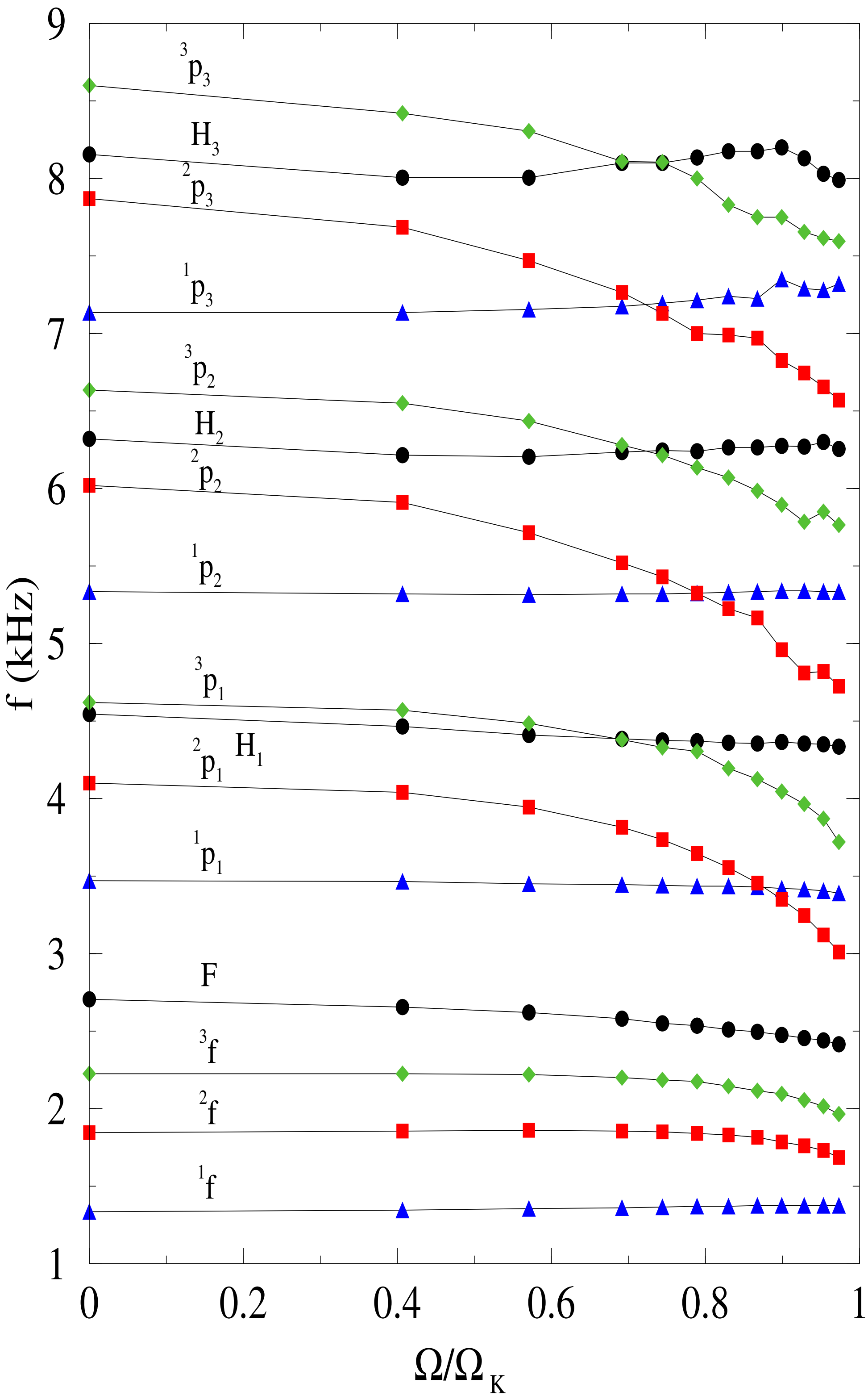

Figure 10: Frequencies of the lowest three quasi-radial modes vs. the ratio of angular velocity of the star Ω to the angular velocity at the mass-shedding limit Ω_K, for the sequence of rotating relativistic stars in Table 1.